Hybrid Patterns and Solitonic Frequency Combs in Non-Hermitian Kerr Cavities

Salim B. Ivars,[1] Carles Milián,[2] Muriel Botey,[1] Ramon Herrero,[1] and Kestutis Staliunas[1,3,4]
[1]*Departament de Física, Universitat Politècnica de Catalunya (UPC), Rambla Sant Nebridi 22, 08222, Terrassa, Barcelona, Catalonia, Spain*
[2]*Institut Universitari de Matemàtica Pura i Aplicada, Universitat Politècnica de València, 46022 València, Spain*
[3]*Institució Catalana de Recerca i Estudis Avançats (ICREA), Passeig Lluís Companys 23, E-08010 Barcelona, Spain*
[4]*Vilnius University, Faculty of Physics, Laser Research Center, Sauletekio Avenue 10, Vilnius, Lithuania*

(Received 10 November 2023; revised 26 June 2024; accepted 24 July 2024; published 29 August 2024)

We unveil a new scenario for the formation of dissipative localized structures in nonlinear systems. Commonly, the formation of such structures arises from the connection of a homogeneous steady state with either another homogeneous solution or a pattern. Both scenarios, typically found in cavities with normal and anomalous dispersion, respectively, exhibit unique fingerprints and particular features that characterize their behavior. However, we show that the introduction of a periodic non-Hermitian modulation in Kerr cavities hybridizes the two established soliton formation mechanisms, embodying the particular fingerprints of both. In the resulting novel scenario, the stationary states acquire a dual behavior, playing the role that was unambiguously attributed to either homogeneous states or patterns. These fundamental findings have profound practical implications for frequency comb generation, introducing unprecedented reversible mechanisms for real-time manipulation.

DOI: 10.1103/PhysRevLett.133.093802

Pattern formation in extended systems is a far-from-equilibrium phenomenon that rules the dynamics of nonlinear physical, chemical, or biological systems [1–6]. The existence and stability of pattern states (PSs), together with that of the so-called flat or homogeneous states (HSs), lies at the core of the dissipative localized structure (LS) formation [7–9], including optical solitons and frequency combs. The emergence of solitons in different regimes of nonlinear systems is generally associated with the existence of two stable solutions, either a PS and HS for anomalous group velocity dispersion (GVD) or two stable HSs for normal GVD. Some nonlinear systems have additionally shown to hold tristability: three different stable HSs [10–12], two PSs, and one HS [13,14] or two HSs and one PS [15–17]. However, the two paradigms of formation of LSs were not found to coexist and the character of the basal states remains unique and well-defined.

In this Letter, we unveil a novel hybrid scenario in the formation of solitons and patterns opening a new avenue in the comprehension of nonlinear systems. Specifically, we demonstrate that the introduction of a periodic modulation in Kerr cavities with normal GVD is qualitatively similar to the effect of Turing instability of the anomalous GVD, in the sense that the modulation introduces low amplitude Turing-like (periodic) states without destabilizing the system. This is the key for the dual and hybridized mechanism that we demonstrate below, which is understood as the blending of the two traditionally separated LS forming regimes. As a result, new families of stable solitons, molecules, and patterns emerge in the normal GVD regime.

In the last two decades, the damped-driven nonlinear Schrödinger equation (NSE) has attracted significant attention [18–22] for the mastering of microcavities and frequency comb generation [23–25]. This model has been demonstrated to accurately describe the evolution of the light field in Kerr resonators. It admits LSs in the two canonical formation regimes associated with normal and anomalous GVD [19,26].

The introduction of inhomogeneities in the damped-driven NSE has been studied through the modulation of external injection or intracavity modulation [27]. In the first case, the soliton dynamics has been studied for temporal modulations of the driving field [28,29], and the introduction of a spatial profile in the injected field has been shown to stabilize LSs [30]. In the second case, phase modulations by electro-optical modulators within the ring cavity have been shown to support synthetic dimensions [31–33] and stabilization of 3D solitons [34].

In parallel, the introduction of non-Hermitian (complex) potentials in nonlinear systems has demonstrated the ability to induce a wide range of intriguing properties: unidirectional couplings arising from potential asymmetries [35,36], stabilization of new solutions [37,38], the support of constant intensity waves [39], the occurrence of exceptional points and jamming anomaly [40], or selective single-mode lasing [41], among others (see, e.g., [42–44] for reviews). In optics, non-Hermitian potentials have been successfully implemented in recent experiments [45,46]. For instance, electro-optical modulators have been shown to effectively modulate the complex refractive index

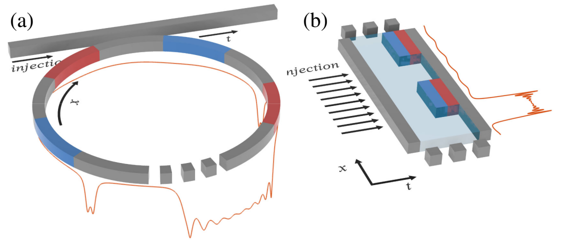

FIG. 1. Schematic representation of possible experimental systems holding hybridized LSs formation. (a) Kerr optical ring cavity with integrated electro-optical modulators for phase and amplitude modulation. (b) Thin Fabry-Perot cavity with $\chi^{(3)}$ medium with loss and phase masks.

with integrated technology [see Fig. 1(a) and Ref. [47] for a recent review, and references therein]. In thin-film Fabry-Perot resonators [48–52], the refractive index and loss modulations can be introduced with spatial phase and loss masks [see Fig. 1(b)]. These cavities have emerged as attractive options for generating frequency combs [53,54]. Despite obvious differences with rings, the nonlinear stationary solutions of both systems share close similarities [53].

The damped-driven NSE modeling passive Kerr dispersive cavities [20–22] can be easily generalized to include a complex potential,

$$\partial_t\psi = -i\partial_x^2\psi - (1+\delta i)\psi + 2i|\psi|^2\psi + V(x)\psi + h,$$
$$V(x) = me^{-i\phi}\cos\left(\frac{2\pi px}{L}\right); \tag{1}$$

see Refs. [31–34] for the derivation of the normalized model and estimation of physical parameters. The cavity-laser detuning δ is our control parameter and the equation includes a third order Kerr nonlinearity, an external energy injection h, and a complex potential $V(x)$. Here, m represents the depth of modulation, p is the number of periods of length L along the cavity path, and ϕ represents the ratio between real and imaginary parts. In this Letter, we fix the number of oscillations to seven without any loss of generality. For details on numerical methods see, e.g., [55,56].

Regarding the formation of LSs, for the homogeneous bistability case (normal GVD), it is well-established that fronts or connections between two HSs typically exhibit one exponential decaying oscillatory tail, and one monotonous connection related to the complex and real eigenvalues associated with each stable state [57,58]. Such an oscillatory tail serves as a potential enabling two fronts to pin to each other, forming a LS. When two fronts are close, the large oscillation amplitude leads to a strong effective potential generating a large coupling interval as a function of the control parameter. Conversely, as the distance between the fronts increases, this interval narrows. Ultimately, the LS can only form when the fronts have null relative velocity, a condition that only occurs for particular values of the parameters (at the Maxwell point). The above ingredients induce a collapsed configuration in the bifurcation structure known as "collapsed snaking" [57]. For the bistability of a PS and a HS (anomalous GVD), the pinning of the two fronts, heteroclinic connections between both states, does not depend on the number of oscillations of the LS close to the PS but on the PS itself. Therefore, the generated branches associated with different LSs span the same interval of the control parameter, leading to what is known as "standard homoclinic snaking." The invariance of the system by a space-reversal symmetry, $x \to -x$, splits the LSs into two disjointed sets with even and odd numbers of oscillations of the pattern, respectively [59–61]. In general, the two snaking diagrams are found in different regimes due to the distinct involved bistable states. These building mechanisms do not coexist, and thus collapsed and standard snake branches are not connected.

Therefore, a natural way to observe the hybridization of the system is by inspecting the bifurcation diagram of these solutions. The study of the curve connected to the homogeneous solutions is summarized in Fig. 2. Importantly, in normal GVD regimes, the stability of the upper homogeneous state is lost by a saddle node (SN) bifurcation. This is opposed to the anomalous GVD where the stability of the HS is lost at a Turing instability (TI) point, arising due to the parametric four-photon mixing. The introduction of the periodic potential takes the role of Turing instability to modulate the system HSs. This induces the system to fold the HS curve, and connect the upper and lower HS with periodic solutions that become stable; see Fig. 2(a). The inset (i) enlarges the branch of the unstable PS for $m = 0$, which emerges from the middle HS; see inset (ii). With the potential, this branch splits into two different solutions: one of them being a stable PS, now connected to the HSs, and the other unstable and now part of a closed loop that derives from the modulation of the middle branch. Note that the branches of the two (stable and unstable) modulated and unmodulated patterns are almost overlapping. Added to this and shown in the insets (ii) and (iii), the middle HS becomes detached from $SN_{1,2}$ and forms an isola or closed loop.

Since the PSs can be understood as a train of solitons, accordingly, the branches follow the expected collapsed organization until the width of a single soliton reaches the width of the period of the modulation. This organizes the discrete periodic structures, P_n, where the label n refers to the position in the collapsed snaking. A crucial effect of the introduction of the potential is the fact that the snaking structure gains a slant. This tilt is a finite-size effect induced by the extra boundary introduced by the potential at each period [62]. Such tilting grows with m, eventually exceeding the HS bistable region; see Figs. 2(a)–2(d). The non-Hermiticity of the potential favors this tilt; see the Supplemental Material [63]. This brings to light the

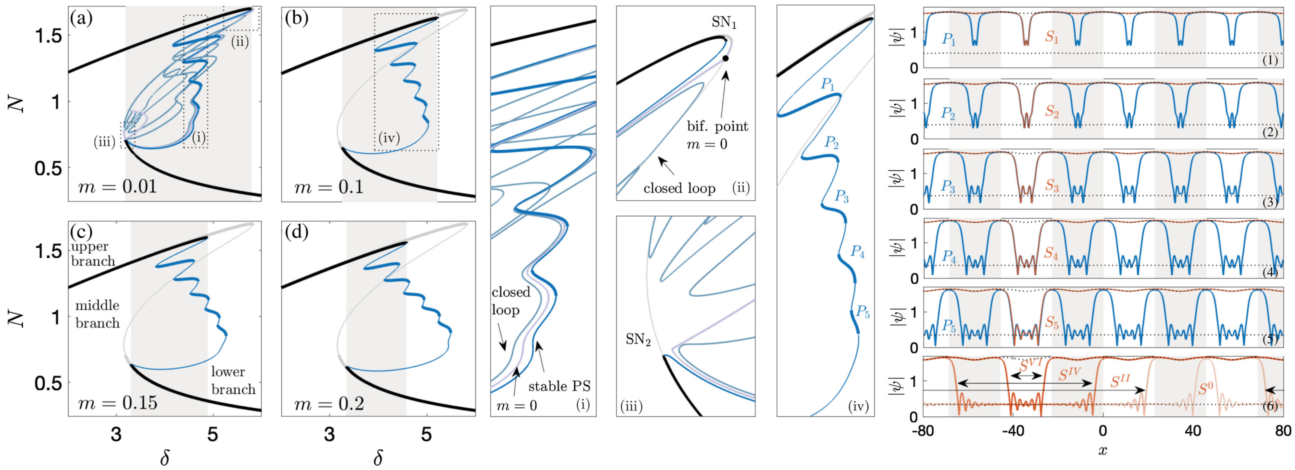

FIG. 2. Bifurcation diagrams of HSs and PSs and corresponding spatial profiles. (a)–(d) Norm$N \equiv 1/L \int_0^L |\Psi(x)| dx$, versus detuning, for increasing values of m, showing the HSs (black) and PSs (blue and turquoise). The thick and thin curves indicate stable or unstable solutions, gray shaded area indicates HS bistability, and the HS (gray) for $m = 0$ is depicted as a reference. Insets (i) and (ii) enlarge the overlap of the unmodulated PS branch (violet), the closed loop (turquoise) evolving from the middle branch, and the stabilized PS (blue); (ii) also shows the SN_1, and the PS bifurcation point for the unmodulated system. Inset (iii) shows the detachment of solutions from SN_2. Inset (iv) highlights the different families of stable PS, labeled as P_n, shown on the right panels along with solitons S_n. The bottom right panel illustrates even solitons, $S^{0-\mathrm{VI}}$, with widths surpassing a single period L; periods are shaded in gray and white. $h = 1.7$.

hybridization and dual character of the system. Parts of the periodic solutions can no longer be understood as a product of the HS bistability but achieve the pattern character. The different families of solutions are displayed in the panels of Fig. 2 and inset (iv), where S_n refers to a single soliton from a particular P_n solution. Whenever the width of the soliton exceeds one period of the modulation, we denote the soliton as S^Q, Q being the number of full oscillations of the upper HS. Importantly, the modulated upper solution now takes the role of a pattern in the formation of LS. Panel (6) in Fig. 2 shows solutions with an even number of oscillations, S^{VI-0}.

In this Letter, multistability of two background solutions and patterns is achieved by the introduction of a modulation. Note that while such background solutions are not strictly homogeneous, the effect of the potential introduces relatively weak modulations; see the dotted curves on panels (1)–(6) in Fig. 2. With the potential, a new hybrid scheme where the basal solutions acquire a dual character is generated and summarized in Fig. 3. The figure captures the complexity and richness of the modulated system, where the typical collapsed and standard homoclinic snaking link. We differentiate two situations depending on whether the PS existence lies only within or exceeds the HS bistable area. In the first case, depicted in Figs. 3(a) and 3(b) for $m = 0.1$, the LS branches containing the different families bifurcate from the two main SNs. In Fig. 3(a) we show the branches of S_n. As for stabilized P_n, their existence is organized in a tilted collapsed snaking until its width exceeds a modulation period. Inspecting this structure, one could conclude that switching waves connecting both quasihomogeneous states are the building blocks of these solutions. Yet, once the P_n existence limit is exceeded, the homogeneous upper solution changes its role to a pattern. Broader solitons with even number of oscillations of the upper state, $S^{0,\mathrm{II},\mathrm{IV}}$, are now organized in a standard homoclinic snaking. This transition happens due to the duality of the upper HS induced by the potential. In turn, Fig. 3(b) provides the analogous situation for even solitons, $S^{\mathrm{I},\mathrm{III},\mathrm{V}}$, also organized in an intertwined homoclinic snaking. This existence (and detachment) of the branches of even and odd solitons highlights that the physics from the case of anomalous GVD is also present in the system. Interestingly, this hybridization enlarges the stability area of bright solitons (for instance $S^{\mathrm{III}-0}$). For no modulation, and without higher order terms, they are found just for the parameters of the Maxwell point [64,65]. Note, on the lower inset, the intricate connection of the branch approaching the SN_2 due to the symmetry of the system. At the top, we show how the odd soliton branch connects to a collapsed snaking structure of a molecule corresponding to two solitons in two neighboring periods $\{S_n, S_n\}$; see the inset and the profiles on the corresponding panels. Solitons can now bond due to the oscillation of the upper state, induced by the potential. Although not shown, stable molecules with different number of solitons, not necessarily laying in neighboring periods, exist and are stable.

An example of a case where the PS exceeds the bistable area is illustrated in Fig. 3(c). As commented earlier, this introduces unequivocally the pattern character to these periodic solutions. In this case, for solitons with even number of oscillations of the upper state, it is interesting to note two different organizations of the bifurcation structures. The previous branch splits. The collapsed snaking

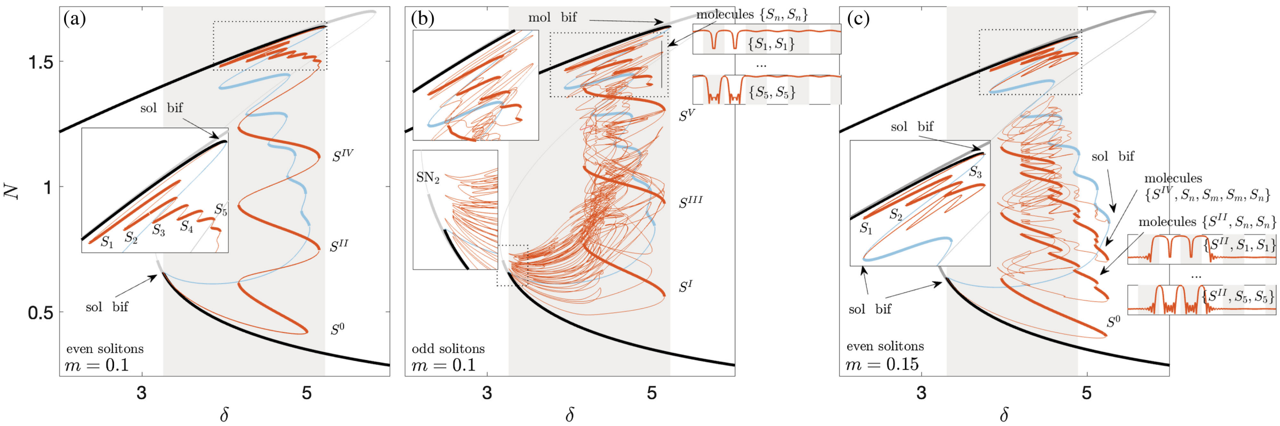

FIG. 3. Bifurcation structure of LSs in different hybridized scenarios. Norm versus detuning diagram of solitonic solutions (orange). (a) Family of even solitons for $m = 0.1$ holding a tilted collapsed snaking followed by a standard homoclinic bifurcation structure. The inset enlarges the narrower soliton states S_n. (b) Family of odd solitons for $m = 0.1$ with an analogous structure but with a collapsed snaking structure of two solitons molecule states of the type $\{S_n, S_n\}$, whose profiles are provided on the panels. Lower-left inset: magnification of the SN_2 of the lower homogeneous solution. (c) Splitting of the even soliton solutions branch. Molecules of the type $\{S^{IV}, S_n, S_m, S_m, S_n\}$ and $\{S^{II}, S_n, S_n\}$, with field profiles provided on the right-hand panels. Inset: enlargement of the collapsed snaking structure of narrow solitons. In all plots, the thick and thin lines indicate stable and unstable states. Periodic solutions of Fig. 2 are included for completeness.

structure of S_n remains, although connecting the upper HS to a PS; see inset. In turn, for broader solitons we can observe a reminiscence of the standard homoclinic snaking surpassing the HS bistable area; see S_0. Moreover, multiple branches of molecule-type solutions develop within the snaking. As an example, these solutions associated with S_0 are of two types. First, solutions of the form $\{S^{\mathrm{II}}, S_n, S_n\}$, containing two narrow solitons S_n within a wide soliton S^{II}. Second, we find solutions $\{S^{\mathrm{IV}}, S_n, S_m, S_m, S_n\}$, containing four solitons. Because of the symmetry of the system, we can have two pairs of different solitons embedded in the upper state of S^{IV}. As expected, cases with $n \neq m$ exist in areas of bistability of P_n and P_m. In this figure, stable solutions are only partially shown to illustrate the complexity and richness of the hybrid system.

The search for real-time manipulation of frequency combs is a crucial property that is being explored in different situations [66–70]. In this Letter, we uncover a mechanism for a deterministic and reversible switch between states with different widths. Such control relies on the tilt of snaking structures of different solutions. This phenomenon is exemplified for solitons S_n as provided in Fig. 4(a). The depicted numerical simulation is performed assuming the stable soliton S_1 as the initial condition. The detuning δ is adiabatically increased in time, up to the value of stability of S_5. Tracking the width of the LS, it is possible to observe the dynamic transition between them. Such transition is rapidly triggered when the different solitons reach their existence limit. Indeed, it is the shift of their existence intervals that allows for the reversible switching

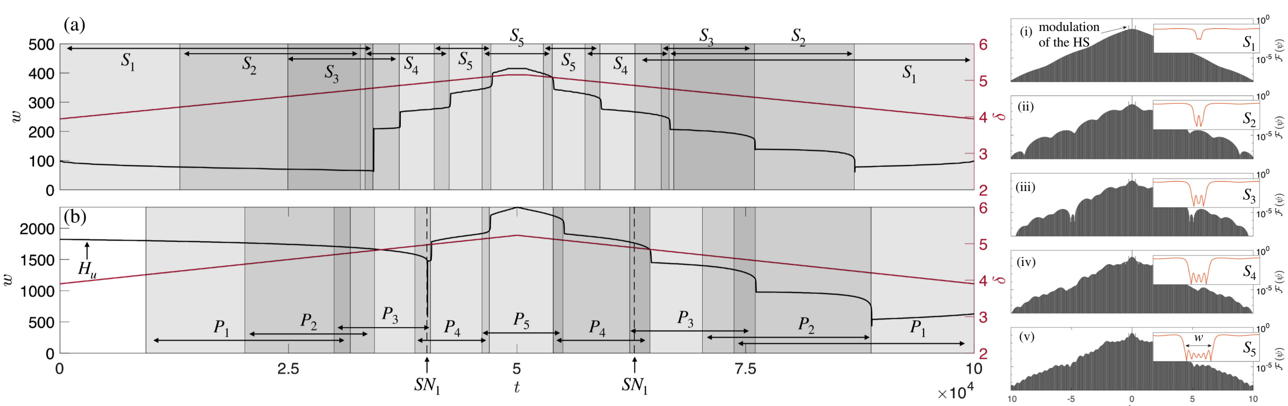

FIG. 4. Temporal manipulation of frequency combs. Dynamical change of full widht at half maximum, w, (black curves) of the propagating field and change of the detuning (red curves), for (a) deterministic transitions between different families of Solitons S_n; (b) turning on the system and switching between different patterns P_n. Shaded areas correspond to stable areas of the different states. Panels (i)–(v) depict stable switchable comb spectra associated to solitons S_{1-5}.

among different solitonic families. Panels (i)–(v) in Fig. 4 show the frequency combs associated to solitons S_{1-5}.

Moreover, for normal GVD cavities, access to the homogeneous bistable area is essential to start the generation of frequency combs. Recently, excitation of dark solitons via self-injection locking has been demonstrated [71,72]. In this Letter, we take advantage of the hybridization of the system that displaces the existence region of some states outside the inaccessible uniform bistable area. The recession of the first SN_1 introduces an access point to the homogeneous bistable area, which can be excited by an adiabatic blue shift of the laser as depicted in Fig. 4(b). The upper homogeneous solution is expected to evolve toward a P_n rather than to the lower HS since the potential has an effect as the Turing instability. Notably, patterns exhibit a deterministic switching mechanism analogous to that observed in solitons.

To conclude, we here present a novel scenario for the formation of localized structures. While it has been long-established that the building blocks for solitons in nonlinear systems are states that are either patterns or flat states, we introduce a most unusual scenario in which the basal states (patterns and flat) acquire a dual behavior so that the system may use one state as "quasiflat" or as a pattern. Throughout this Letter, such duality is discussed in the context of a driven dissipative cavity with normal GVD, described by the damped-driven NSE, under the introduction of a periodic non-Hermitian modulation. The reported results represent a general new paradigm to understand the formation of nonlinear localized structures, where physics from normal and anomalous GVD regimes blend. In particular, this unconventional hybridized scenario gives birth to an extraordinarily rich landscape where many different species of frequency combs coexist, being stable and accessible. Furthermore, the hybridization of the LS formation scheme has important practical consequences for real-time reshaping of combs. Beyond the fundamental reported findings, these results pave the route for flexible frequency comb generation.

Acknowledgments—This work was supported by the Spanish government via PID2022-138321NB-C21 and Generalitat de Catalunya via 2021 SGR 00606; C. M. acknowledges PID2021-124618NB-C21, funded by MCIN/ AEI/10.13039/501100011033 and "ERDF: a way of making Europe" of the European Union, and Generalitat Valenciana via PROMETEO/2021/082.

[1] M. C. Cross and P. C. Hohenberg, Rev. Mod. Phys. **65**, 851 (1993).
[2] F. T. Arecchi, S. Boccaletti, and P. Ramazza, Phys. Rep. **318**, 1 (1999).
[3] K. Staliunas and V. J. Sanchez-Morcillo, *Transverse Patterns in Nonlinear Optical Resonators* (Springer Science & Business Media, Heidelberg, Germany, 2003), Vol. 183.
[4] L. Lugiato, F. Prati, and M. Brambilla, *Nonlinear Optical Systems* (Cambridge University Press, Cambridge, England, 2015).
[5] A. M. Turing, Bull. Math. Biol. **52**, 153 (1990).
[6] E. Knobloch, Conmatphys. **6**, 325 (2015).
[7] B. Schäpers, M. Feldmann, T. Ackemann, and W. Lange, Phys. Rev. Lett. **85**, 748 (2000).
[8] E. Meron, Phys. Rep. **218**, 1 (1992).
[9] Y. Pomeau, Physica (Amsterdam) **23D**, 3 (1986).
[10] Y. Dumeige and P. Féron, Phys. Rev. A **84**, 043847 (2011).
[11] M. Anderson, Y. Wang, F. Leo, S. Coen, M. Erkintalo, and S. G. Murdoch, Phys. Rev. X **7**, 031031 (2017).
[12] C. Milián, Y. V. Kartashov, D. V. Skryabin, and L. Torner, Opt. Lett. **43**, 979 (2018).
[13] M. Tlidi, M. Georgiou, and P. Mandel, Phys. Rev. A **48**, 4605 (1993).
[14] L. Spinelli, G. Tissoni, M. Brambilla, F. Prati, and L. A. Lugiato, Phys. Rev. A **58**, 2542 (1998).
[15] Y. R. Zelnik, P. Gandhi, E. Knobloch, and E. Meron, Chaos **28**, 033609 (2018).
[16] F. Al Saadi and A. Champneys, Phil. Trans. R. Soc. A **379**, 20200277 (2021).
[17] P. Parra-Rivas, A. Champneys, F. Al-Sahadi, D. Gomila, and E. Knobloch, arXiv:2208.04009.
[18] D. J. Kaup and A. C. Newell, Phil. Trans. R. Soc. A **361**, 413 (1978).
[19] I. V. Barashenkov and Y. S. Smirnov, Phys. Rev. E **54**, 5707 (1996).
[20] Y. K. Chembo and C. R. Menyuk, Phys. Rev. A **87**, 053852 (2013).
[21] L. A. Lugiato and R. Lefever, Phys. Rev. Lett. **58**, 2209 (1987).
[22] M. Haelterman, S. Trillo, and S. Wabnitz, Opt. Commun. **91**, 401 (1992).
[23] H. Bao, L. Olivieri, M. Rowley, S. T. Chu, B. E. Little, R. Morandotti, D. J. Moss, J. S. T. Gongora, M. Peccianti, and A. Pasquazi, Phys. Rev. Res. **2**, 023395 (2020).
[24] V. Brasch, M. Geiselmann, T. Herr, G. Lihachev, M. H. Pfeiffer, M. L. Gorodetsky, and T. J. Kippenberg, Science **351**, 357 (2016).
[25] T. J. Kippenberg, R. Holzwarth, and S. A. Diddams, Science **332**, 555 (2011).
[26] A. Matsko, A. Savchenkov, and L. Maleki, Opt. Lett. **37**, 43 (2012).
[27] F. Copie, M. Conforti, A. Kudlinski, A. Mussot, and S. Trillo, Phys. Rev. Lett. **116**, 143901 (2016).
[28] C. Todd, Z. Li, S. Coen, S. G. Murdoch, G.-L. Oppo, and M. Erkintalo, Phys. Rev. A **107**, 013506 (2023).
[29] I. Hendry, W. Chen, Y. Wang, B. Garbin, J. Javaloyes, G.-L. Oppo, S. Coen, S. G. Murdoch, and M. Erkintalo, Phys. Rev. A **97**, 053834 (2018).
[30] F. Tabbert, T. Frohoff-Hülsmann, K. Panajotov, M. Tlidi, and S. V. Gurevich, Phys. Rev. A **100**, 013818 (2019).
[31] A. K. Tusnin, A. M. Tikan, and T. J. Kippenberg, Phys. Rev. A **102**, 023518 (2020).
[32] N. Englebert, N. Goldman, M. Erkintalo, N. Mostaan, S.-P. Gorza, F. Leo, and J. Fatome, Nat. Phys. **19**, 1014 (2023).
[33] A. Dutt, Q. Lin, L. Yuan, M. Minkov, M. Xiao, and S. Fan, Science **367**, 59 (2020).

[34] Y. Sun, P. Parra-Rivas, C. Milián, Y. V. Kartashov, M. Ferraro, F. Mangini, R. Jauberteau, F. R. Talenti, and S. Wabnitz, Phys. Rev. Lett. **131**, 137201 (2023).

[35] S. B. Ivars, M. Botey, R. Herrero, and K. Staliunas, Chaos, Solitons Fractals **165**, 112774 (2022).

[36] M. N. Akhter, S. B. Ivars, M. Botey, R. Herrero, and K. Staliunas, Phys. Rev. Lett. **131**, 043604 (2023).

[37] S. B. Ivars, M. Botey, R. Herrero, and K. Staliunas, Chaos, Solitons Fractals **168**, 113089 (2023).

[38] W. W. Ahmed, S. Kumar, J. Medina, M. Botey, R. Herrero, and K. Staliunas, Opt. Lett. **43**, 2511 (2018).

[39] K. G. Makris, Z. H. Musslimani, D. N. Christodoulides, and S. Rotter, Nat. Commun. **6**, 7257 (2015).

[40] I. Barashenkov, D. Zezyulin, and V. Konotop, New J. Phys. **18**, 075015 (2016).

[41] L. Feng, Z. J. Wong, R.-M. Ma, Y. Wang, and X. Zhang, Science **346**, 972 (2014).

[42] Y. Ashida, Z. Gong, and M. Ueda, Adv. Phys. **69**, 249 (2020).

[43] V. V. Konotop, J. Yang, and D. A. Zezyulin, Rev. Mod. Phys. **88**, 035002 (2016).

[44] S. V. Suchkov, A. A. Sukhorukov, J. Huang, S. V. Dmitriev, C. Lee, and Y. S. Kivshar, Laser Photonics Rev. **10**, 177 (2016).

[45] Ş. K. Özdemir, S. Rotter, F. Nori, and L. Yang, Nat. Mater. **18**, 783 (2019).

[46] D. Cheng, E. Lustig, K. Wang, and S. Fan, Light Sci. Appl. **12**, 158 (2023).

[47] Y. Hu, D. Zhu, S. Lu, X. Zhu, Y. Song, D. Renaud, D. Assumpcao, R. Cheng, C. Xin, M. Yeh *et al.*, arXiv: 2404.06398.

[48] L. A. Lugiato and F. Prati, Phys. Rev. Lett. **104**, 233902 (2010).

[49] X. Hachair, S. Barland, L. Furfaro, M. Giudici, S. Balle, J. R. Tredicce, M. Brambilla, T. Maggipinto, I. M. Perrini, G. Tissoni *et al.*, Phys. Rev. A **69**, 043817 (2004).

[50] M. Brambilla, L. Lugiato, and M. Stefani, Europhys. Lett. **34**, 109 (1996).

[51] U. Peschel, D. Michaelis, and C. O. Weiss, IEEE J. Quantum Electron. **39**, 51 (2003).

[52] M. Brambilla, L. A. Lugiato, F. Prati, L. Spinelli, and W. J. Firth, Phys. Rev. Lett. **79**, 2042 (1997).

[53] D. C. Cole, A. Gatti, S. B. Papp, F. Prati, and L. Lugiato, Phys. Rev. A **98**, 013831 (2018).

[54] T. Wildi, M. A. Gaafar, T. Voumard, M. Ludwig, and T. Herr, Optica **10**, 650 (2023).

[55] J. Hult, J. Lightwave Technol. **25**, 3770 (2007).

[56] C. Milián, Y. V. Kartashov, D. V. Skryabin, and L. Torner, Phys. Rev. Lett. **121**, 103903 (2018).

[57] Y.-P. Ma, J. Burke, and E. Knobloch, Physica (Amsterdam) **239D**, 1867 (2010).

[58] P. Parra-Rivas, E. Knobloch, D. Gomila, and L. Gelens, Phys. Rev. A **93**, 063839 (2016).

[59] D. Avitabile, D. J. Lloyd, J. Burke, E. Knobloch, and B. Sandstede, SIAM J. Appl. Dyn. Syst. **9**, 704 (2010).

[60] J. Burke and E. Knobloch, Chaos **17**, 037102 (2007).

[61] M. Tlidi, P. Mandel, and R. Lefever, Phys. Rev. Lett. **73**, 640 (1994).

[62] G. Kozyreff, P. Assemat, and S. J. Chapman, Phys. Rev. Lett. **103**, 164501 (2009).

[63] See Supplemental Material at http://link.aps.org/supplemental/10.1103/PhysRevLett.133.093802 for hybridisation scheme of the two canonical soliton formation mechanisms occurring with normal Group Velocity Dispersion for potentials deviating from an ideal harmonic function and effect of the non-hermiticity.

[64] M. Tlidi and L. Gelens, Opt. Lett. **35**, 306 (2010).

[65] P. Parra-Rivas, D. Gomila, and L. Gelens, Phys. Rev. A **95**, 053863 (2017).

[66] Y. He, Q.-F. Yang, J. Ling, R. Luo, H. Liang, M. Li, B. Shen, H. Wang, K. Vahala, and Q. Lin, Optica **6**, 1138 (2019).

[67] E. Nazemosadat, A. Fülöp, Ó. B. Helgason, P.-H. Wang, Y. Xuan, D. E. Leaird, M. Qi, E. Silvestre, A. M. Weiner, and V. Torres-Company, Phys. Rev. A **103**, 013513 (2021).

[68] J. H. Talla Mbé, C. Milián, and Y. K. Chembo, Eur. Phys. J. D **71**, 1 (2017).

[69] S. B. Ivars, Y. V. Kartashov, L. Torner, J. A. Conejero, and C. Milián, Phys. Rev. Lett. **126**, 063903 (2021).

[70] S. B. Ivars, Y. V. Kartashov, P. F. de Córdoba, J. A. Conejero, L. Torner, and C. Milián, Nat. Photonics **17**, 767 (2023).

[71] H. Wang, B. Shen, Y. Yu, Z. Yuan, C. Bao, W. Jin, L. Chang, M. A. Leal, A. Feshali, M. Paniccia *et al.*, Phys. Rev. A **106**, 053508 (2022).

[72] W. Jin, Q.-F. Yang, L. Chang, B. Shen, H. Wang, M. A. Leal, L. Wu, M. Gao, A. Feshali, M. Paniccia *et al.*, Nat. Photonics **15**, 346 (2021).